Available online at www.sciencedirect.com
SCIENCE DIRECT®
Computer Physics Communications 153 (2003) 71–84
Computer Physics Communications
www.elsevier.com/locate/cpc

Smoothed particle hydrodynamics: Applications to heat conduction

J.H. Jeong [a], M.S. Jhon [a,*], J.S. Halow [b], J. van Osdol [b]

[a] *Department of Chemical Engineering, Carnegie Mellon University, Pittsburgh, PA 15213, USA*
[b] *National Energy Technology Laboratories, Morgantown, WV 26507, USA*

Received 18 March 2002; received in revised form 6 January 2003; accepted 6 January 2003

Abstract

In this paper, we modify the numerical steps involved in a smoothed particle hydrodynamics (SPH) simulation. Specifically, the second order partial differential equation (PDE) is decomposed into two first order PDEs. Using the ghost particle method, consistent estimation of near-boundary corrections for system variables is also accomplished. Here, we focus on SPH equations for heat conduction to verify our numerical scheme. Each particle carries a physical entity (here, this entity is temperature) and transfers it to neighboring particles, thus exhibiting the mesh-less nature of the SPH framework, which is potentially applicable to complex geometries and nanoscale heat transfer. We demonstrate here only 1D and 2D simulations because 3D codes are as simple to generate as 1D codes in the SPH framework. Our methodology can be extended to systems where the governing equations are described by PDEs.

PACS: 02.60.Lj; 02.70.Rw; 11.10.Ef; 44.10.+i

Keywords: Smoothed particle hydrodynamics; Heat conduction; Boundary conditions

1. Introduction

The smoothed particle hydrodynamics (SPH) is a mesh-less, transient, Lagrangian technique historically developed for astrophysical applications [1,2]. The inherent benefit of the SPH formulation is the transformation of complex partial differential equations (PDEs) into their corresponding ordinary differential equations (ODEs) via construction of integral equations with a smoothing (kernel) function. This transformation is an advantage to scientists and engineers especially in the realm of parallel computations. Recently, SPH has grown into a successful and respected simulation tool. In particular, the mesh-less nature of SPH provides us with a potentially powerful tool for complicated 3D geometries (3D codes are as simple to generate as 1D codes). Randle and Libersky [3] presented an excellent review of the advantages and recent progress in SPH. Li and Liu [4] surveyed recent developments of mesh-free and particle methods, and SPH was selected as the most promising candidate.

* Corresponding author.
E-mail address: mj3a@andrew.cmu.edu (M.S. Jhon).

0010-4655/03/$ – see front matter
doi:10.1016/S0010-4655(03)00155-3

Although SPH has been successful in a broad spectrum of engineering applications, several stumbling blocks are yet to be overcome. Among these challenges, boundary condition implementation is a very subtle yet difficult issue. The logical difficulty lies in the fact that SPH was invented primarily to deal with astrophysical problems where no system boundary exists. However, in many emerging technology applications, the influence of boundaries is of the utmost importance. It should be emphasized that the physical boundary of a system domain does not coincide with the SPH interaction boundary. Therefore, if the cut-off region of the SPH interaction range is not carefully estimated, near-boundary deficiencies inevitably occur. To remedy this situation, Taketa et al. [5] proposed the ghost particle method, in which some particles are located outside the system boundary but are included in the SPH interaction range. They applied this method to the second order PDE, and it inevitably involved the manipulation of the second derivative of the kernel function.

The heat conduction problem provides us with an excellent test example to verify a SPH formulation and computational algorithm. Here, temperature is assigned to each particle such that the particles carry the physical entity of temperature and transfer it to the neighboring particles, thus highlighting the mesh-less nature of SPH. If convection is included, it has the potential to treat the Lagrangian framework systematically. Surprisingly, there have been only a few attempts to solve the conduction equation via SPH methods. Chen et al. [6] solved the heat conduction problem via a corrective kernel method, where the kernel itself is reproduced by a linear corrective function near the boundary. They used the Taylor series expansion to estimate the kernel and provided a systematic algorithm to resolve the particle deficiency near the boundary. Because they applied their method to the second derivative, they used the second order derivative of the kernel function. Our treatment is different.

The purpose of this work is to develop a systematic algorithm for SPH formulation that takes the boundary condition implementation into account. Furthermore, the novelty of our approach is that it decomposes a second order PDE into two first order PDEs; one is a balance equation (exact) and the other is a constitutive equation (approximate). This decomposition could provide us with an advantage in handling multiphase systems, where different constitutive equations generally apply to each phase. Using the ghost particle method, we achieve a consistent estimation of near-boundary corrections for system variables. The methodology developed here for the heat conduction problem can be systematically extended to solve other classes of PDEs, which include fluid flow [7,8] and nanoscale heat transfer [9] by adopting proper constitutive equations. We treat the velocity or temperature-specified boundary condition as the Dirichlet-type boundary condition, and the stress or heat flux-specified boundary condition as the Neumann-type boundary condition. To verify our numerical procedure, we compare the SPH results with the exact solution for the 1D case, and with the numerical solution obtained via finite difference method (FDM) for 2D case. Our efforts and initial success in these near-boundary corrections enhance the understanding of SPH fundamentals and pave the road for a full-scale SPH simulation, where boundary corrections play a dominant role in determining the accuracy of the PDE solution.

2. SPH representation of heat conduction equation

The concept behind SPH is based on an interpolation scheme. The smoothed function value for any physical quantity $f(\mathbf{x}_i)$ is defined by

$$f_i \equiv f(\mathbf{x}_i) \equiv \int_{\Gamma} f(\mathbf{x}) W(\mathbf{x}-\mathbf{x}_i, h)\,\mathrm{d}\mathbf{x} \equiv \int_{\Gamma} \Pi(\mathbf{x}-\mathbf{x}_i, h)\,\mathrm{d}\mathbf{x}, \tag{1}$$

which has second order accuracy with respect to the SPH interaction parameter h. Here, $\mathbf{x}$ and $\mathbf{x}_i$ are position vectors and W is a kernel function. As illustrated in Fig. 1, $\mathbf{x}_i$ is located at the center of Γ, implying an interaction domain with respect to $\mathbf{x}_i$. In this figure, the system domain and interaction domain are denoted by Ω and Γ, and $\partial\Omega$ and $\partial\Gamma$ represent their boundaries. Eq. (1) is the kernel representation to average functional distribution. It should satisfy the properties listed below.

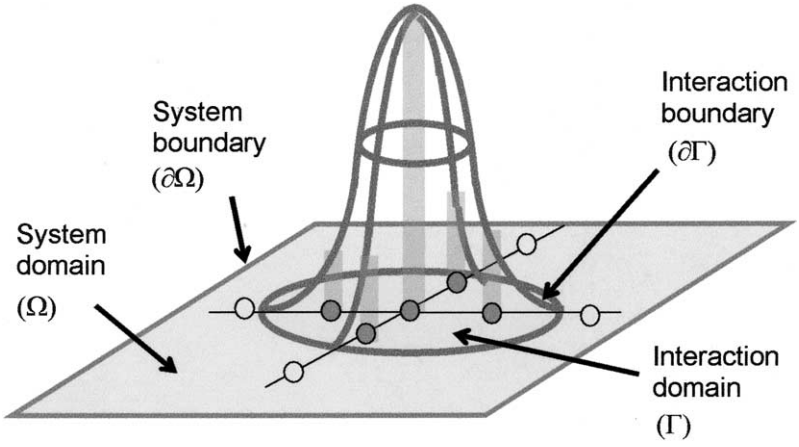

Fig. 1. A schematic to demonstrate SPH interaction in system domain.

(i) Positivity: $W(\mathbf{x}, h) \geqslant 0,$ (2)

(ii) Normalization: $\int_\Gamma W(\mathbf{x}, h)\,\mathrm{d}\mathbf{x} = 1,$ (3)

(iii) Surface property: $W(\mathbf{x}, h)|_{\partial\Gamma} = \nabla W(\mathbf{x}, h)|_{\partial\Gamma} = \nabla\nabla W(\mathbf{x}, h)|_{\partial\Gamma} = 0.$ (4)

From Eq. (4), we obtain

$$\int_\Gamma \nabla W(\mathbf{x}, h)\,\mathrm{d}\mathbf{x} = 0. \tag{5}$$

For simplicity's sake, we use the 2D Lucy's kernel [1], represented by

$$W(\mathbf{x}, h) = \frac{5}{4\pi h^2}\left(1 + \frac{3|\mathbf{x}|}{2h}\right)\left(1 - \frac{|\mathbf{x}|}{2h}\right)^3 H\left(2 - \frac{|\mathbf{x}|}{h}\right). \tag{6}$$

Here $H(\xi)$ is the Heaviside function, defined by

$$H(\xi) \equiv \begin{cases} 1 & \text{if } \xi \geqslant 0, \\ 0 & \text{if } \xi < 0. \end{cases} \tag{7}$$

Eq. (1) can be approximated by the following:

$$f_i = \sum_{j=1}^{N} \frac{f_j}{n_j} W(\mathbf{x}_i - \mathbf{x}_j) \equiv \sum_{j=1}^{N} \frac{f_j}{n_j} W_{ij} \equiv \sum_{j=1}^{N} \frac{\Pi_{ij}}{n_j}. \tag{8}$$

Here, i and j are the particle indices, N the number of the particles, and n_j the number density of the jth particles. Eq. (8) is the particle representation, and provides us with a tool for discretization. From Eqs. (1) and (8), the continuum field variables, $f(\mathbf{x})$, can be cast into discrete particle variables f_i.

Fig. 2 illustrates a schematic for the SPH approximations: (a) smoothing by kernel representation, and (b) discretizing by particle representation. The particle approximation is basically a quadrature formula in the integration procedure. This particle approximation is the simplest numerical integration method and may result in a global deterioration of accuracy.

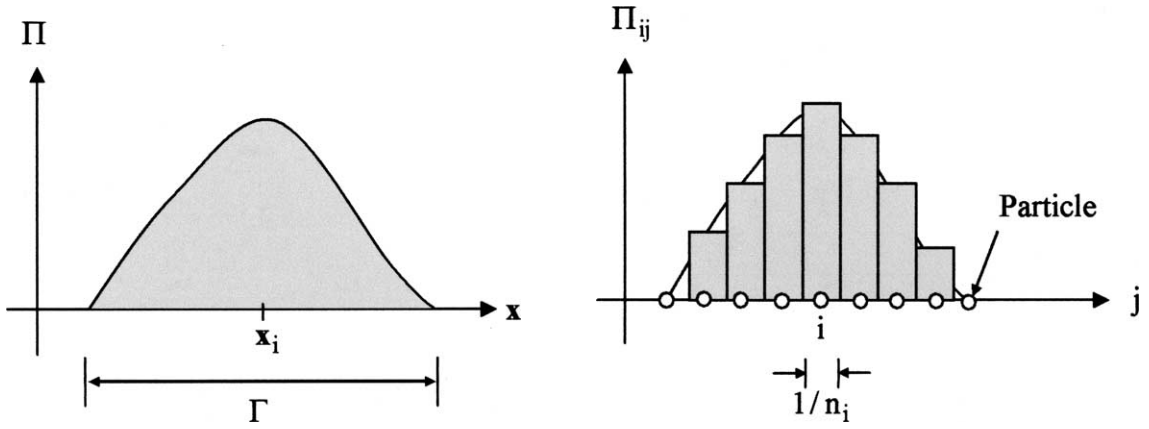

(a) (b)

Fig. 2. SPH concepts: (a) smoothing by kernel and (b) discretizing by particle representations.

Spatial derivatives can be transformed into their corresponding SPH interaction equations via integration by parts. For example, by using the kernel property (iii) or Eq. (4), we have

$$(\nabla f)_i = \int_\Gamma \big(\nabla f(\mathbf{x})\big) W(\mathbf{x}-\mathbf{x}_i, h)\,\mathrm{d}\mathbf{x} = -\int_\Gamma f(\mathbf{x}) \nabla W(\mathbf{x}-\mathbf{x}_i, h)\,\mathrm{d}\mathbf{x}. \tag{9}$$

By applying the particle approximation given in Eq. (8), we have

$$(\nabla f)_i = -\sum_{j=1}^{N} \frac{f_j}{n_j} (\nabla W)_{ij} \equiv \sum_{j=1}^{N} \frac{f_j}{n_j} \frac{\mathbf{x}_{ij}}{r_{ij}} \frac{\mathrm{d}W(r_{ij})}{\mathrm{d}r_{ij}}. \tag{10}$$

Here,

$$\mathbf{x}_{ij} \equiv \mathbf{x}_j - \mathbf{x}_i, \qquad r_{ij} \equiv |\mathbf{x}_{ij}|. \tag{11}$$

Since our formulation deals with two first order PDEs rather than one second order PDE, Eqs. (1) and (10) are the key equations in transforming a PDE-based heat conduction equation into an ODE-based one.

Two first order PDEs are the energy balance equation and the constitutive equation. In dimensionless form, these equations are given by:

$$\frac{\mathrm{D}T}{\mathrm{D}t} = -\nabla \cdot \mathbf{q}, \tag{12}$$

$$\mathbf{q} = -\alpha \nabla T, \tag{13}$$

where $\mathrm{D}/\mathrm{D}t \equiv \partial/\partial t + \mathbf{v} \cdot \nabla$ is the material or Stokes' derivative, $\mathbf{q}$ is heat flux, T is temperature, and α is thermal diffusivity. We set $\alpha = 1$ throughout the paper without loss of generality. The traditional SPH formulation uses the second order PDE by combining Eqs. (12) and (13). However, our formulation consists of two first order PDEs, i.e.

$$\frac{\mathrm{d}T_i}{\mathrm{d}t} = \int_\Gamma \mathbf{q} \cdot \nabla W\,\mathrm{d}\mathbf{x}, \tag{14}$$

$$\mathbf{q}_i = \int_\Gamma T \nabla W\,\mathrm{d}\mathbf{x}. \tag{15}$$

In order to satisfy conservation law, Eqs. (14) and (15) are modified via Eq. (5):

$$\frac{\mathrm{d}T_i}{\mathrm{d}t} = \int_{\Gamma} (\mathbf{q} + \mathbf{q}_i) \cdot \nabla W \, \mathrm{d}\mathbf{x}, \tag{16}$$

$$\mathbf{q}_i = \int_{\Gamma} (T - T_i) \nabla W \, \mathrm{d}\mathbf{x}. \tag{17}$$

Note that the positive and negative signs in Eqs. (16) and (17) are unimportant when the particles have symmetric distributions. For heat conduction alone, the particles' positions are stationary, however, in dealing with convection, the position's symmetry cannot be maintained, and this broken symmetry requires modification in order to conserve energy. By applying Eqs. (8) and (9) to Eqs. (16) and (17), we obtain the SPH interaction equations for heat conduction, given by

$$\frac{\mathrm{d}T_i}{\mathrm{d}t} = \sum_{j=1}^{N} \frac{1}{n_j} (\mathbf{q}_i + \mathbf{q}_j) \cdot \frac{\mathbf{x}_{ij}}{r_{ij}} \frac{\mathrm{d}W_{ij}}{\mathrm{d}r_{ij}}, \tag{18}$$

$$\mathbf{q}_i = \sum_{j=1}^{N} \frac{1}{n_j} (T_j - T_i) \frac{\mathbf{x}_{ij}}{r_{ij}} \frac{\mathrm{d}W_{ij}}{\mathrm{d}r_{ij}}. \tag{19}$$

Note that among the kernel's properties, Eq. (5) is important when estimating particle interactions that are revealed in Eqs. (18) and (19), while Eq. (3) is important when evaluating the number density.

3. Boundary condition implementation

The system boundary ($\partial\Omega$) does not coincide with the SPH interaction boundary ($\partial\Gamma$) because $\partial\Gamma$ is always circular in contrast to the arbitrarily-shaped $\partial\Omega$. In other words, the SPH interaction region is not boundary-fitted, which is an important characteristic in a structured grid generation.

Fig. 3 shows a schematic of the near-boundary deficiency in an SPH picture. Note that the system boundary splits the interaction range Γ into the domains $(\Gamma \cap \Omega)$ and $\widehat{\Gamma} \equiv \Gamma - (\Gamma \cap \Omega)$. That is, when the center particle

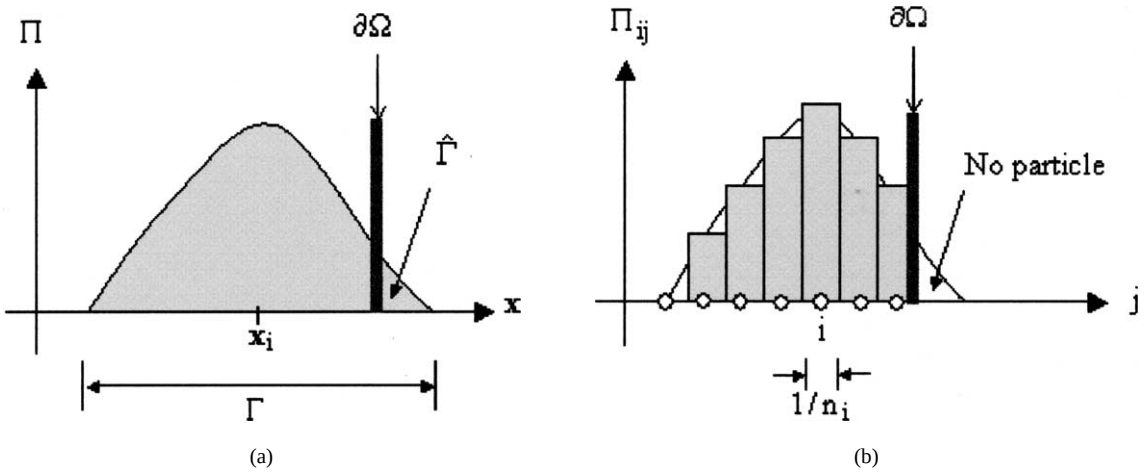

Fig. 3. SPH interaction domain near system boundary: (a) smoothing by kernel and (b) discretizing by particle representation.

is located near the system boundary, the interaction domain has a cut-off region approximately equal to the system boundary. Thus, if the cut-off region is not accurately estimated, near-boundary deficiencies inevitably appear. Because particles are generated only within Ω, the particle approximation of Eq. (8) is no longer valid in $\widehat{\Gamma}$. That is,

$$f_i = \sum_{j=1}^{N} \frac{f_j}{n_j} W_{ij} + \int_{\widehat{\Gamma}} f(\mathbf{x}) W(\mathbf{x} - \mathbf{x}_i, h)\, \mathrm{d}\mathbf{x}. \tag{20}$$

Note that to evaluate Eq. (20), we need the value for f in $\widehat{\Gamma}$.

By extrapolating, the function value $f(\mathbf{x})$ can be expressed as

$$f = f_i + \frac{r}{r_b}(f_b - f_i) + \mathrm{o}(h^2) \cong \left(1 - \frac{r}{r_b}\right) f_i + \frac{r}{r_b} f_b, \tag{21}$$

where f_b denotes function values at $\mathbf{x}_b$. The vector $(\mathbf{x} - \mathbf{x}_i)$ intersects $\partial\Omega$ at $\mathbf{x}_b$, and

$$r \equiv |\mathbf{x} - \mathbf{x}_i|, \qquad r_b \equiv |\mathbf{x}_b - \mathbf{x}_i|. \tag{22}$$

By substituting Eq. (21) into Eq. (20), we have

$$f_i = \sum_{j=1}^{N} \frac{f_j}{n_j} W_{ij} + f_i \int_{\widehat{\Gamma}} \left(1 - \frac{r}{r_b}\right) W(\mathbf{x} - \mathbf{x}_i)\, \mathrm{d}\mathbf{x} + \int_{\widehat{\Gamma}} f_b \frac{r}{r_b} W(\mathbf{x} - \mathbf{x}_i)\, \mathrm{d}\mathbf{x}. \tag{23}$$

By rearranging Eq. (23), we have

$$f_i = \frac{\sum_{j=1}^{N} \frac{f_j}{n_j} W_{ij} + \int_{\widehat{\Gamma}} f_b \frac{r}{r_b} W(\mathbf{x} - \mathbf{x}_i)\, \mathrm{d}\mathbf{x}}{1 - \int_{\widehat{\Gamma}} (1 - \frac{r}{r_b}) W(\mathbf{x} - \mathbf{x}_i)\, \mathrm{d}\mathbf{x}}. \tag{24}$$

If the functional form of f_b is given, we can obtain f_i, since the kernel is a function of position only.

We often encounter a difficulty in evaluating Eq. (24) when the boundary function value f_b should be simultaneously determined by internal values as a part of the solution, i.e.

$$\lim_{\mathbf{x}_i \to \mathbf{x}_b} f(\mathbf{x}_i) \equiv f(\mathbf{x}_b) \equiv f_b. \tag{25}$$

In the case of number density n_i, the particles are generated solely inside the system domain, and thus the number density at the boundary is determined by taking a limiting value of Eq. (25).

When the boundary value f_b is not explicitly given, we approximate it as f_i by assuming that $r/r_b \ll 1$. That is,

$$f_b \cong f_i. \tag{26}$$

Note that this assumption improves as the interaction parameter h becomes small. By substituting Eq. (26) into Eq. (24), we have

$$f(\mathbf{x}_i) = \frac{\sum_{j=1}^{N} (f_j/n_j) W_{ij}}{1 - \int_{\widehat{\Gamma}} W(\mathbf{x} - \mathbf{x}_i)\, \mathrm{d}\mathbf{x}}. \tag{27}$$

Consequently, the number density n_i can be obtained by setting f in Eq. (27) to n.

$$n_i = \frac{\sum_{j=1}^{N} W_{ij}}{1 - \int_{\widehat{\Gamma}} W(\mathbf{x} - \mathbf{x}_i)\, \mathrm{d}\mathbf{x}}. \tag{28}$$

Takeda et al. [5] derived an expression similar to Eq. (28) for the near-boundary density calculation. In this paper, we generalize the ghost particle approach of Takeda et al. to calculate the temperature and heat flux.

Eqs. (18) and (19) are modified by

$$\frac{\mathrm{d}T_i}{\mathrm{d}t} = \sum_{j=1}^{N} \frac{1}{n_j} (\mathbf{q}_i + \mathbf{q}_j) \cdot (\nabla W)_{ij} + \int_{\widehat{\Gamma}} (\mathbf{q} + \mathbf{q}_i) \cdot \nabla W \, \mathrm{d}\mathbf{x}, \tag{29}$$

$$\mathbf{q}_i = \sum_{j=1}^{N} \frac{1}{n_j} (T_j - T_i)(\nabla W)_{ij} + \int_{\widehat{\Gamma}} (T - T_i) \nabla W \, \mathrm{d}\mathbf{x}. \tag{30}$$

By extrapolation, the function values of T and $\mathbf{q}$ in $\widehat{\Gamma}$ can be approximated by setting f in Eq. (21) to T and $\mathbf{q}$.

$$T = T_i + \frac{r}{r_b}(T_b - T_i) + \mathrm{o}(h^2), \tag{31}$$

$$\mathbf{q} = \mathbf{q}_i + \frac{r}{r_b}(\mathbf{q}_b - \mathbf{q}_i) + \mathrm{o}(h^2). \tag{32}$$

By substituting Eqs. (31) and (32) into Eqs. (29) and (30), we have

$$\frac{\mathrm{d}T_i}{\mathrm{d}t} = \sum_{j=1}^{N} \frac{1}{n_j} (\mathbf{q}_i + \mathbf{q}_j) \cdot (\nabla W)_{ij} + \int_{\widehat{\Gamma}} \left(2\mathbf{q}_i + \frac{r}{r_b}(\mathbf{q}_b - \mathbf{q}_i) \right) \cdot \nabla W \, \mathrm{d}\mathbf{x}, \tag{33}$$

$$\mathbf{q}_i = \sum_{j=1}^{N} \frac{1}{n_j} (T_j - T_i)(\nabla W)_{ij} + \int_{\widehat{\Gamma}} \frac{r}{r_b} (T_b - T_i) \nabla W \, \mathrm{d}\mathbf{x}. \tag{34}$$

We consider two simple boundary conditions: a Dirichlet-type boundary condition ($T|_{\partial\Omega} = T_b$) and a Neumann-type boundary condition ($\mathbf{e}_n \cdot \mathbf{q}|_{\partial\Omega} = \mathbf{e}_n \cdot \mathbf{q}_b$). Here, we define the unit normal and tangential vectors at $\partial\Omega$ by $\mathbf{e}_n$ and $\mathbf{e}_t$, respectively. At the Dirichlet-type boundary, T_b is given explicitly, but $\mathbf{q}_b$ is not. From Eq. (26) $\mathbf{q}_b$ becomes $\mathbf{q}_i$. On the other hand, at the Neumann-type boundary, $\mathbf{e}_n \cdot \mathbf{q}_b$ is given explicitly, but T_b and $\mathbf{e}_t \cdot \mathbf{q}_b$ are not. Therefore, $T_b \cong T_i$ and $\mathbf{e}_t \cdot \mathbf{q}_b \cong \mathbf{e}_t \cdot \mathbf{q}_i$.

Consequently, we have

(a) Dirichlet-type boundary:

$$\frac{\mathrm{d}T_i}{\mathrm{d}t} = \sum_{j=1}^{N} \frac{1}{n_j} (\mathbf{q}_i + \mathbf{q}_j) \cdot (\nabla W)_{ij} + 2\mathbf{q}_i \cdot \int_{\widehat{\Gamma}} \nabla W(\mathbf{x} - \mathbf{x}_i) \, \mathrm{d}\mathbf{x}, \tag{35}$$

$$\mathbf{q}_i = \sum_{j=1}^{N} \frac{1}{n_j} (T_j - T_i)(\nabla W)_{ij} + \int_{\widehat{\Gamma}} \frac{r}{r_b} (T_b - T_i) \nabla W(\mathbf{x} - \mathbf{x}_i) \, \mathrm{d}\mathbf{x}; \tag{36}$$

(b) Neumann-type boundary:

$$\begin{aligned} \frac{\mathrm{d}T_i}{\mathrm{d}t} &= \sum_{j=1}^{N} \frac{1}{n_j} (\mathbf{q}_i + \mathbf{q}_j) \cdot (\nabla W)_{ij} \\ &\quad + \int_{\widehat{\Gamma}} \left(\left(\mathbf{q}_i (2 - r/r_b) + \mathbf{q}_b \right) \cdot \mathbf{e}_n \mathbf{e}_n + 2\mathbf{q}_i \cdot \mathbf{e}_t \mathbf{e}_t \right) \cdot \nabla W(\mathbf{x} - \mathbf{x}_i) \, \mathrm{d}\mathbf{x}, \end{aligned} \tag{37}$$

$$\mathbf{q}_i = \sum_{j=1}^{N} \frac{1}{n_j} (T_j - T_i)(\nabla W)_{ij}. \tag{38}$$

4. Results and discussion

4.1. Comparison with an exact solution in 1D heat conduction

In order to verify our SPH interaction equations, we will compare our results to the analytical solution for the 1D heat conduction case. 1D expressions for Eqs. (18) and (19) are:

$$\frac{\mathrm{d}T_i}{\mathrm{d}t} = \sum_{j=1}^{N} \frac{W'_{ij}}{n_j}(q_j + q_i)\big(2H(x_j - x_i) - 1\big), \tag{39}$$

$$q_i = \sum_{j=1}^{N} \frac{W'_{ij}}{n_j}(T_j - T_i)\big(2H(x_j - x_i) - 1\big), \tag{40}$$

where $W'_{ij} \equiv \mathrm{d}W_{ij}/\mathrm{d}r_{ij}$. Here the 1D Lucy's kernel and its derivative are given by

$$W_{ij} = 5/(2 + 3r_{ij}/h)(2 - r_{ij}/h)^3 H(2 - r_{ij}/h)/128h, \tag{41}$$

$$W'_{ij} = -15(r_{ij}/h)(2 - r_{ij}/h)^2 H(2 - r_{ij}/h)/32h^2. \tag{42}$$

Note that $W_{ij} \geqslant 0$ and $W'_{ij} \leqslant 0$ for arbitrary r_{ij}. The kth particle contribution to the ith particle can be expressed by

$$\left(\frac{\mathrm{d}T_i}{\mathrm{d}t}\right)_k = \frac{W'_{ik}}{n_k}(q_k + q_i)\big(2H(x_k - x_i) - 1\big), \tag{43}$$

$$(\mathbf{q}_i)_k = \frac{W'_{ik}}{n_k}(T_k - T_i)\big(2H(x_k - x_i) - 1\big). \tag{44}$$

For $x_k > x_i$, the positive value of $(q_k + q_i)$ yields $(\mathrm{d}T_i/\mathrm{d}t)_k < 0$, implying that the net outgoing heat flux causes the temperature to decrease. On the other hand, for $x_k < x_i$, the positive value of $(q_k + q_i)$ yields $(\mathrm{d}T_i/\mathrm{d}t)_k > 0$ because the incoming heat flux causes the temperature to increase. Also the negative definite property of W'_{ij} in Eq. (44) ensures that heat is always transmitted from high-temperature particles to low-temperature particles, thus satisfying the second law of thermodynamics.

From Eqs. (12) and (13), $T(x,t)$ is governed by

$$\frac{\partial T}{\partial t} = \frac{\partial^2 T}{\partial x^2}, \tag{45}$$

with initial and boundary conditions: $T(x,0) = T_0$, $T(0,t) = T_0$, and $T(1,t) = T_1$. In this case, the analytical solution is given by

$$T(x,t) = T_0 + (T_1 - T_0)x + 2(T_1 - T_0)\sum_{j=1}^{\infty} \frac{(-1)^j}{\lambda_j} \exp\big(-\lambda_j^2 t\big) \sin(\lambda_j x), \tag{46}$$

where $\lambda_j = \pi j$.

Fig. 4 shows the comparison, where we set $T_0 = 0$, $T_1 = 1$, and $h = 2r_{ij}$. The solid lines in the figure denote the analytical solution of Eq. (46) and symbols denote SPH solutions. Fig. 4(a) shows the SPH solution using 50 particles. From the figure, we find that the SPH solution deviates slightly from the exact solution near the boundary $x = 1$, particularly early on. Interestingly, as time elapses the numerical errors near $x = 1$ settle down without accumulation. Fig. 4(b) shows that the SPH result becomes more accurate simply by increasing the number of particles to 500. In order to display the results clearly, only 50 particles are exhibited in the figure. By comparing the SPH solution with the analytical solution, we find excellent agreement between them.

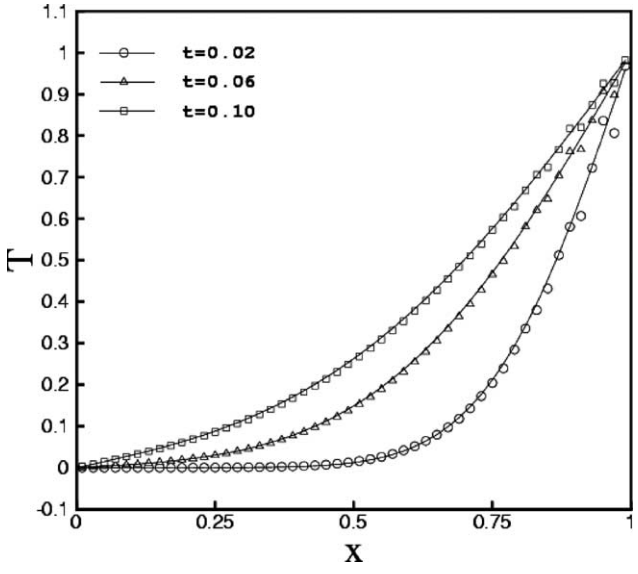

(a)

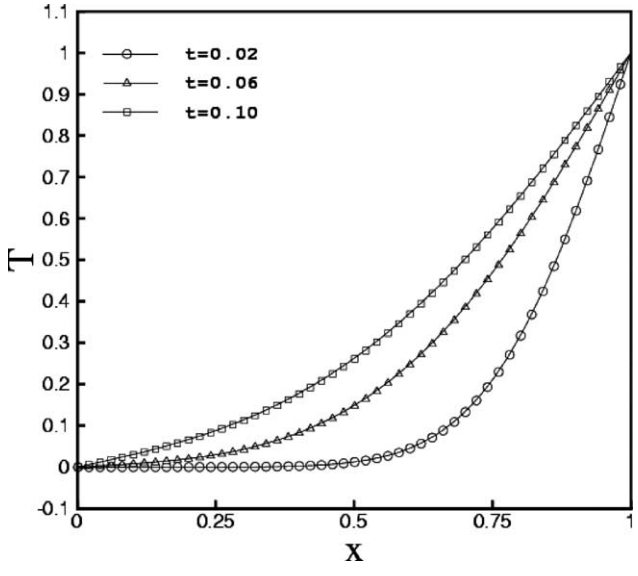

(b)

Fig. 4. Comparison of SPH results with the analytical solution for 1D heat conduction: (a) $N = 50$ and (b) $N = 500$.

4.2. Comparison with numerical solutions by the Finite Difference Method (FDM) in 2D heat conduction

In this section, SPH formulation is applied to the 2D heat conduction case with a simple rectangular geometry. In order to verify our numerical procedure, we also analyze an identical problem via FDM. By combining Eqs. (12) and (13), we obtain the governing equation in a 2D Cartesian coordinate for $T = T(x, y; t)$,

$$\frac{\partial T}{\partial t} = \frac{\partial^2 T}{\partial x^2} + \frac{\partial^2 T}{\partial y^2}, \tag{47}$$

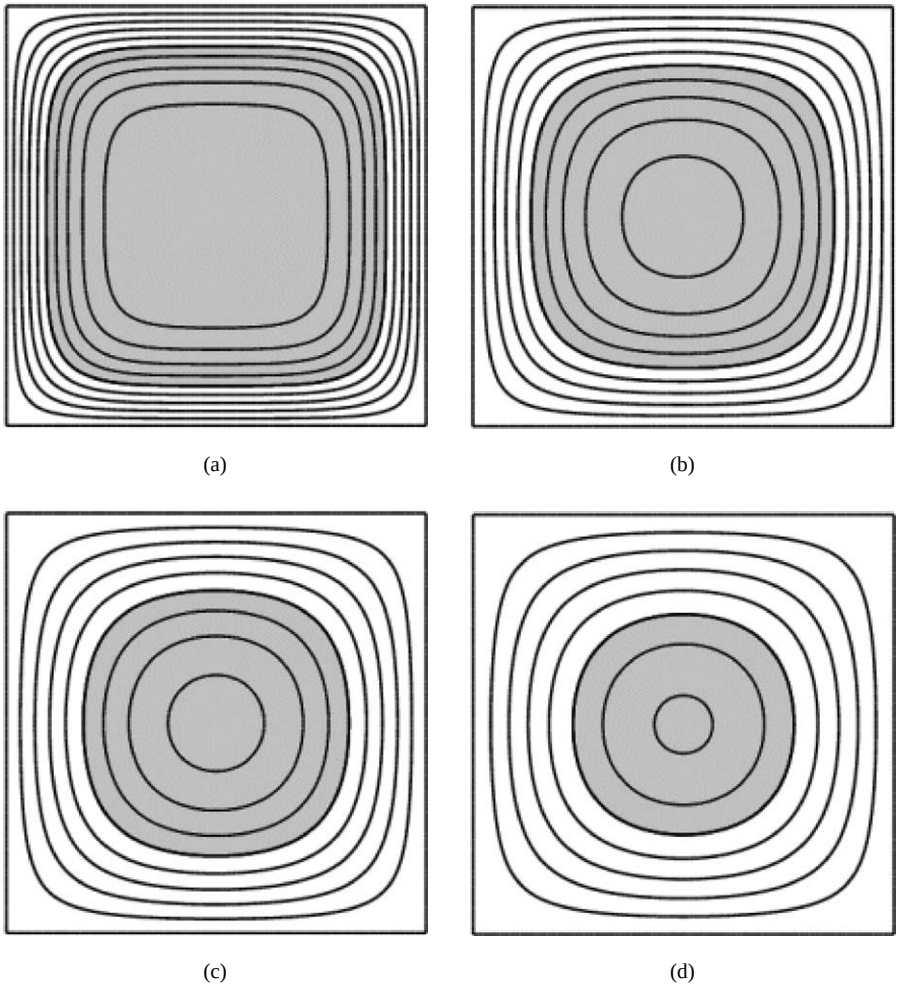

Fig. 5. Temperature profiles obtained by FDM for the case that all of the boundaries have Dirichlet-type conditions: (a) $t = 0.01$, (b) $t = 0.02$, (c) $t = 0.03$, and (d) $t = 0.04$.

with the initial condition of

$$T(x, y; 0) = T_0.$$

In FDM analysis, we discretize the system domain ($0 \leqslant x \leqslant 1, 0 \leqslant y \leqslant 1$) by

$$x = i/40, \quad i = 0, \ldots, 40, \tag{48}$$

$$y = j/40, \quad j = 0, \ldots, 40. \tag{49}$$

In our SPH computation, we generate uniformly distributed particles by placing them at the center of each cell made by Eqs. (48) and (49). Thus, 1600 particles are generated in the system domain. The interaction parameter h is given by $h = 2r_{ij}$.

First we examine the case where every boundary has a Dirichlet-type condition, given by

$$T(0, y; t) = T(1, y; t) = T(x, 0; t) = T(x, 1; t) = T_1. \tag{50}$$

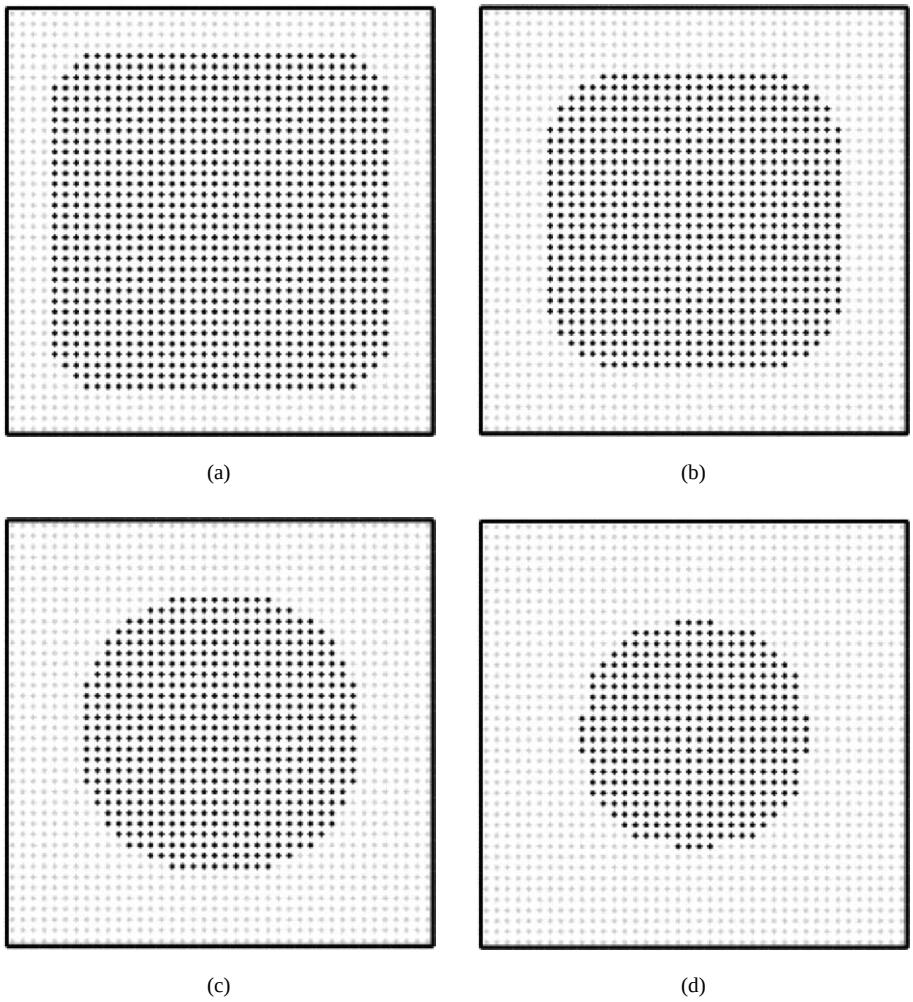

Fig. 6. Temperature profiles obtained by SPH for the case that all of the boundaries have Dirichlet-type conditions: (a) $t = 0.01$, (b) $t = 0.02$, (c) $t = 0.03$, and (d) $t = 0.04$.

Fig. 5 shows the temperature contours at a given time, obtained by FDM. Here, we set $T_0 = -1$ and $T_1 = 1$, and use the time step $\Delta t = 10^{-4}$ for numerical integrations. In this figure, the difference between adjacent contours is 0.2. The variables have negative values in the gray regions. As a result of the hot boundaries, initially cold temperatures in the system domain eventually increase. Fig. 6 shows the results obtained via SPH simulation, where dark and light particles represent negative and positive temperatures, respectively. We see that the negative temperature area gradually diminishes due to the conductive transport from the boundary. From the fact that zero temperature location exactly coincides with the calculation obtained from FDM, we conclude that there is quantitative agreement between SPH and FDM results.

Figs. 7 and 8 show FDM and SPH results when no heat flux is allowed at the top plate. We have a Neumann-type condition at $y = 1$, given by

$$\frac{\partial T(x, 1; t)}{\partial y} = 0. \tag{51}$$

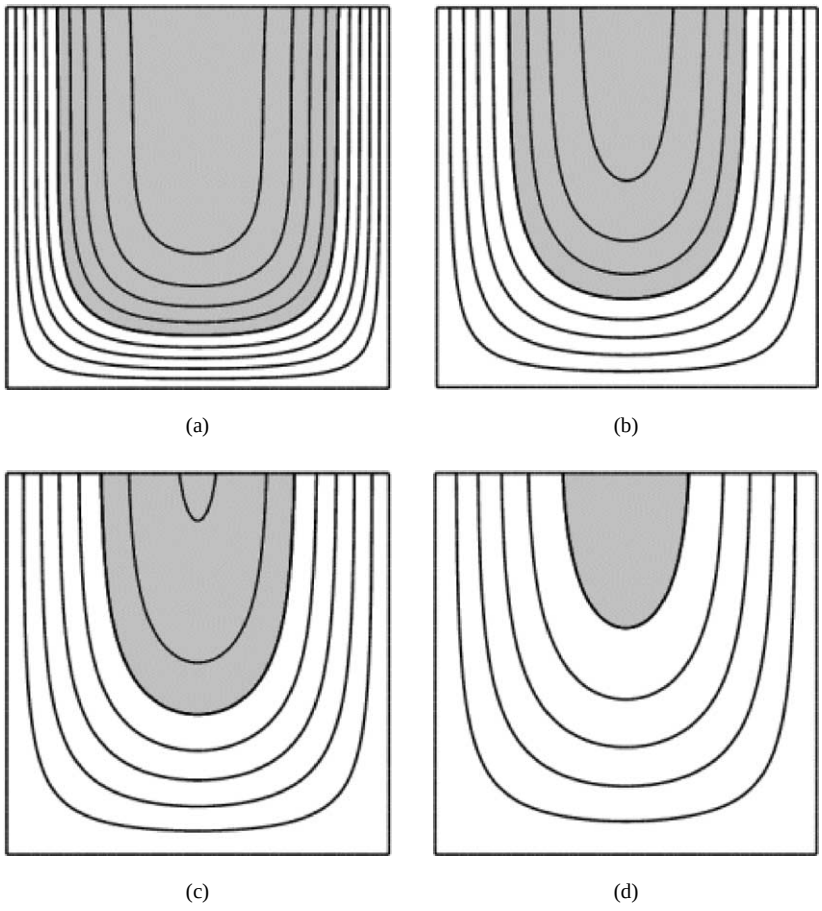

Fig. 7. Temperature profiles obtained by FDM for the case that Neumann-type boundary condition is applied only at top plate: (a) $t = 0.02$, (b) $t = 0.04$, (c) $t = 0.06$, and (d) $t = 0.08$.

Other boundaries conditions are still Dirichlet-type, i.e.,

$$T(0, y; t) = T(1, y; t) = T(x, 0; t) = 1. \tag{52}$$

Due to the boundary condition at $y = 1$, the temperature contours at the top plate become orthogonal to the tangential lines of the boundary. By comparing Figs. 5 and 6 and Figs. 7 and 8, we conclude that our SPH results give excellent agreement with standard FDM analysis.

Fig. 9 demonstrates the SPH computation containing irregular system geometry problem with Dirichlet boundary condition. Comparing with Figs. 5 and 6, the shape of system geometry is changed while the other parameters such as thermal diffusivity are kept the same. Here, the difference between adjacent contours is 0.4. As shown in Fig. 9, the isothermal contours have similar shapes as that of the system boundary, especially at the initial stages. Since implementation of a Neumann boundary condition is just as simple, further analysis will not be presented. For all of these cases, we chose the thermal diffusivity to be equal to one, implying that time is dimensionless.

Note that there is an optimal value of the SPH interaction parameter h. If h becomes incrementally smaller, the number of activated neighbor particles also decreases. For example, when $h \leqslant \min(r_{ij})$, no neighboring jth particles interact with the ith particle. On the other hand, as h gets incrementally larger, more neighboring particles are activated. However, because the SPH formulation is based on $O(h^2)$ accuracy, an excessively high

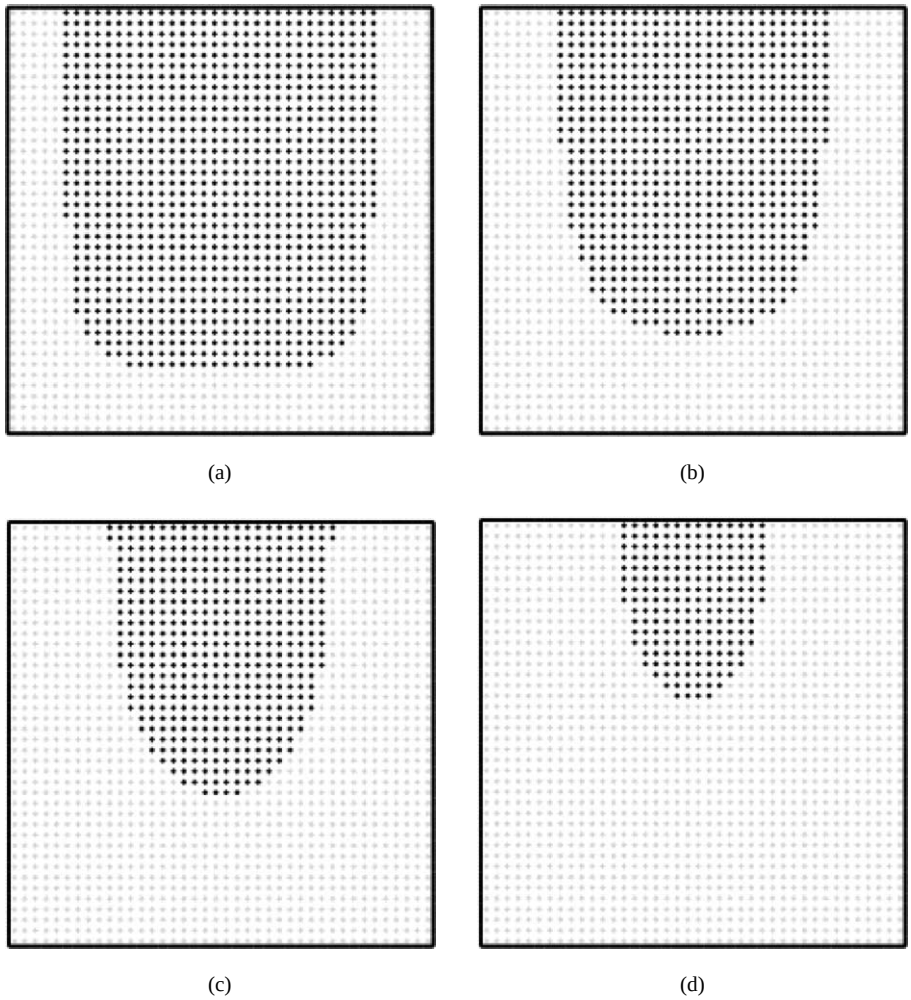

Fig. 8. Temperature profiles obtained by SPH for the case that Neumann-type boundary condition is applied only at top plate: (a) $t = 0.02$, (b) $t = 0.04$, (c) $t = 0.06$, and (d) $t = 0.08$.

interaction parameter h could result in the accumulation of numerical errors or unnecessary computational effort. Consequently, the SPH interaction parameter h, as well as the kernel, should be carefully selected.

5. Conclusions

A systematic and consistent algorithm for SPH formulation is proposed, taking the boundary condition implementation into account. Based on the ghost particle method, consistent estimation of near-boundary corrections for system variables is accomplished by decomposing a second order PDE into two first order PDEs. Our SPH formulation is applied to heat conduction where temperature is assigned to each particle. The methodology developed here can be extended to systems described by PDEs, including Newtonian fluid flow and nanoscale heat transfer in arbitrarily-shaped geometries. Our efforts and initial success in obtaining a consistent

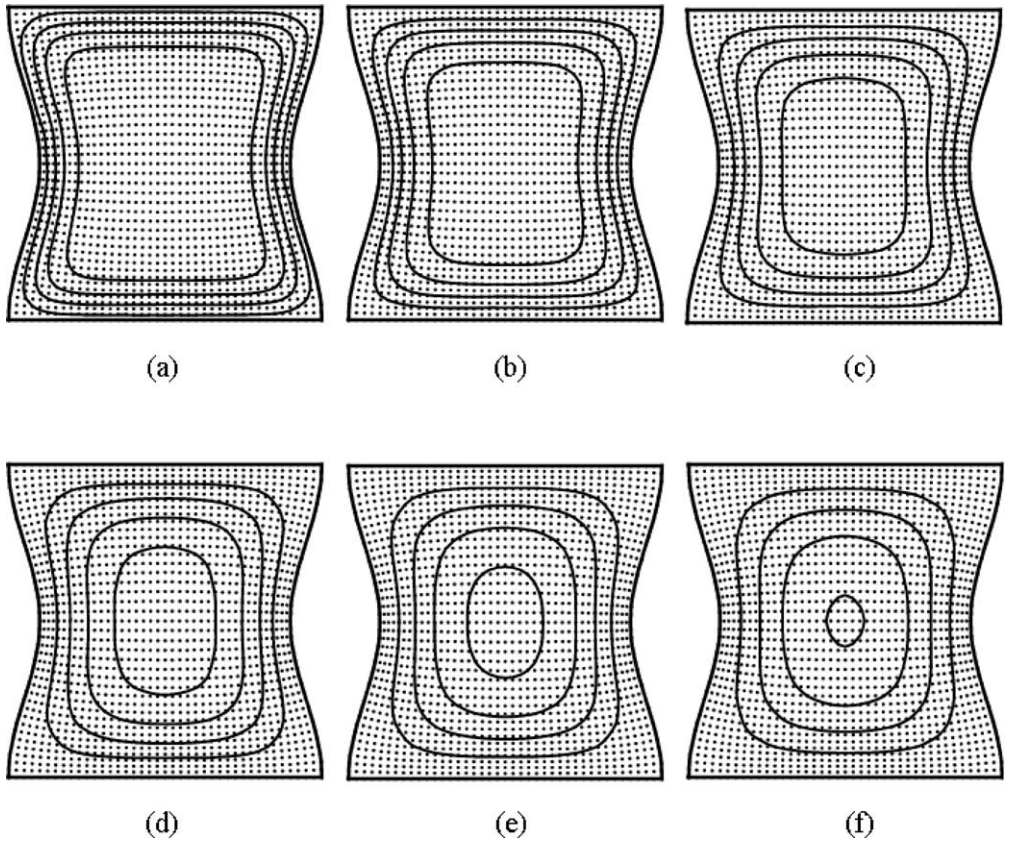

Fig. 9. Temperature profiles obtained by SPH for the case of irregular system geometry with Dirichlet boundary condition: (a) $t = 0.004$, (b) $t = 0.008$, (c) $t = 0.012$, (d) $t = 0.016$, (e) $t = 0.020$, and (f) $t = 0.024$.

algorithm for near-boundary corrections will eventually enhance the understanding of SPH fundamentals and pave the road for full-scale, particle-based numerical simulation in transport process.

References

[1] L.B. Lucy, A numerical approach to testing of the fission hypothesis, Astron. J. 82 (1977) 1013.
[2] R.A. Gingold, J.J. Monaghan, Smoothed particle hydrodynamics: theory and application to non-spherical stars, Monthly. Nat. R. Astron. Soc. 181 (1977) 375.
[3] P.W. Randle, L.D. Libersky, Smoothed particle hydrodynamics: some recent improvements and application, Appl. Mech. Engrg. 139 (1996) 375.
[4] S. Li, W.K. Liu, Meshfree and particle methods and their applications, Appl. Mech. Rev. 55 (2002) 1.
[5] H. Takeda, S. Miyama, M. Sekiya, Numerical simulation of viscous flow by smoothed particle hydrodynamics, Prog. Theor. Phys. 92 (1994) 939.
[6] J.K. Chen, J.E. Beraun, T.C. Carney, A corrective smoothed particle method for boundary value problems in heat conduction, Int. J. Numer. Methods Engrg. 46 (1999) 231.
[7] J.P. Morris, P.J. Fox, Y. Zhu, Modelling low Reynolds number incompressible flows using SPH, J. Comput. Phys. 136 (1997) 214.
[8] J.J. Monaghan, A. Kocharyan, SPH simulation of multiphase flow, Comput. Phys. Commun. 87 (1995) 225.
[9] D.Y. Tzou, K.S. Chin, Temperature-dependent thermal lagging in ultrafast laser heating, Int. J. Heat Mass Transfer 44 (2001) 1725.